Supplementary Materials for "Quantum Transport across Amorphous-Crystalline Interfaces in Tunnel Oxide Passivated Contact Solar Cells: Direct versus Defect-Assisted Tunneling"

Feng Li(李峰)[1,2*], Weiyuan Duan(端伟元)[2], Manuel Pomaska[2], Malte Köhler[2], Kaining Ding(丁凯宁) [2], Yong Pu(普勇)[1]*, Urs Aeberhard[2], Uwe Rau[2]

[1] *College of Science, Nanjing University of Posts and Telecommunications, Nanjing, Jiangsu, 210023, China*

[2] *IEK-5 Photovoltaik, Forschungszentrum Jülich, 52425 Jülich, Germany.*

[*]Supported by National Natural Science Foundation of China (No. 61704083, 61874060), Natural Science Foundation of Jiangsu Province (No. BK20181388) and NUPTSF (No. NY219030). The authors gratefully acknowledge the computing time granted by the VSR commission on the supercomputer JURECA at Forschungszentrum Jülich.

%Email: lifeng@njupt.edu.cn; puyong@njupt.edu.cn

Theoretical details

The electronic ground states are described in terms of localized orbitals in the form of maximally-localized Wannier functions (MLWFs).[1] Due to the associated linear scaling of required computing time, the MLWFs method is especially effective in simulating a realistically sized device structure.[2-3] The Wannier-function Hamiltonian can be obtained by a Fourier transform from reciprocal space into real space for any arbitrary *k* point, as follows:

$$H_{mn}(k) = \sum_{R} e^{ik\cdot R} H_{mn}(R) \tag{1}$$

Then, the resulting Hamiltonian matrices can be diagonalized to find energy eigenvalues. Since the unitary transformations mix the energy bands at each *k* point, any arbitrary choice of states inside a prescribed window will affect the localization properties of WFs unless energy gaps effectively separate the manifold of interest from higher and lower bands. Thus, an additional disentanglement procedure is introduced to solve this problem,[4] by extracting the best possible manifold of a given dimension from the states falling in a predefined energy window.

Using the Hamiltonian matrices calculated in the last step, the zero-temperature conductance spectrum is computed using the Landauer formula[5] as implemented in the WanT code[6]:

$$C = \frac{2e^2}{h} T(E_f) \tag{2}$$

where *C* is the conductance, *T* is the transmission function, and E_f is the Fermi energy. $2e^2/h$ is the quantum unit of conductance, where *h* is the Planck's constant and *e* is the electronic charge. It represents the probability that an electron injects at one end and transmits to the other end.

The transmission function is expressed in terms of the Green's function of the conductor and

the couplings of the conductor to the leads using the Fisher and Lee formula[7]:

$$T = T_r[\Gamma_L G^r \Gamma_R G^a] \tag{3}$$

Here, $G^r$and G^a are the retarded and advanced Green's functions of the conductor. Γ_L and Γ_R are the functions that describe the coupling of the conductor to the leads. There are two modes for computing the transmittance: two-terminal mode the bulk mode. For the two-terminal mode, all of the information contained in the Hamiltonian is needed, including the on-site Hamiltonian of the conductor (H00_C) and of left/right leads (H00_L and H00_R), the hopping Hamiltonian of left/right leads (H01_L and H01_R), and the coupling between lead and conductor (H_LC and H_CR); while for the bulk mode, only H00_C and H_CR are required.

Finally, the total conductance can be computed. Since all the details of the electronic structure are included in the Hamiltonian matrix, all of the density state for the tunneling transport are automatically considered when computing the transmission spectrum. This integrated method allows for a direct link between the nature of the chemical bonds and the electronic transport properties of the device, providing insight into the mechanisms that govern electron flow at the nanoscale.

Crystalline silicon. We first consider the structural, electronic and transport properties of ideal bulk *c*–Si in order to verify the correctness of the integrated simulation approach. A unit cell containing 8 silicon atoms is used, with a lattice constant of 5.46 Å. The optimized Si–Si bond is 2.35 Å, matching well with the experimental result of ~2.35 Å. The computed electronic band structure of *c*–Si is shown in Fig. S1.

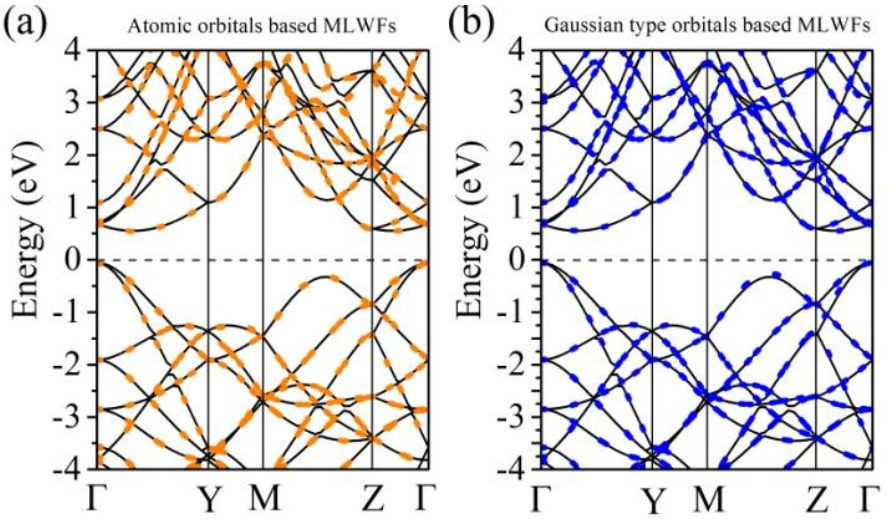

Fig. S1. Band structure of bulk crystalline silicon. The interpolated Wannier band structure based on a set of (a) atomic orbitals, and (b) one-, two-Gaussian type orbitals are depicted in orange and blue dots, respectively. The black lines represent the first-principles band structure based on the Bloch states. The Fermi level is set at 0 eV, indicated as a black dashed line. All the results are computed at the PBE level.

To achieve a linear scaling of required computing time, the electron Bloch wavefunctions, obtained from the *ab initio* calculation, are translated into the MLWF forms through a unitary transformation. The band structure is calculated based on the Hamiltonian as represented in a basis

of MLWFs. Since the choice of a suitable set of Wannier functions is the key to construct the accurate Hamiltonian matrix, we applied two widely used sets of Wannier functions as initial functions: a set of atomic orbitals and a set of one-, two- Gaussian type orbitals. The results are compared and plotted in Fig. S1ab as orange and blue dots, respectively. To check the accuracy of the MLWFs method, the electronic band structure of *c*–Si based on Bloch wavefunctions is also computed and displayed as solid black lines. The chosen set of MLWFs reproduces the band structure of *c*–Si very well. It exhibits a clear indirect band gap of 0.60 eV, which is very close to the DFT result of 0.61 eV. This result proves that the MLWFs method conserves the accuracy of the first-principles electronic structure calculations, confirming the reliability of the integrated method used in this work. Since the accuracy is very similar for atomic orbitals and Gaussian-type orbitals, while the former costs ~30 % less memory than the latter, we thus used atomic orbitals as initial Wannier functions for MLWFs in all of the computations.

We then calculated the conductance for bulk *c*–Si by bulk model. The transport is computed by interpolating the in-plane *k* points as integrated into the WanT codes. We found that *c*–Si has a clear transmission gap of 0.62 eV (Fig. S2b). This value agrees well with the computed electrical band gap of 0.61 eV, which is also consistent with the result of the density of states (Fig. S2a). The quantum conductance is a constant proportional to the number of transmitting channels available for charge mobility, which are equal to the number of bands at the same energy. This result indicates a one-to-one correspondence between the band structure and the quantum conductance spectrum for *c*–Si. On the other hand, for the amorphous-crystalline interfaces, the conductance will display a large complex that is related to the channel DOS and contact DOS, which is discussed in the next section.

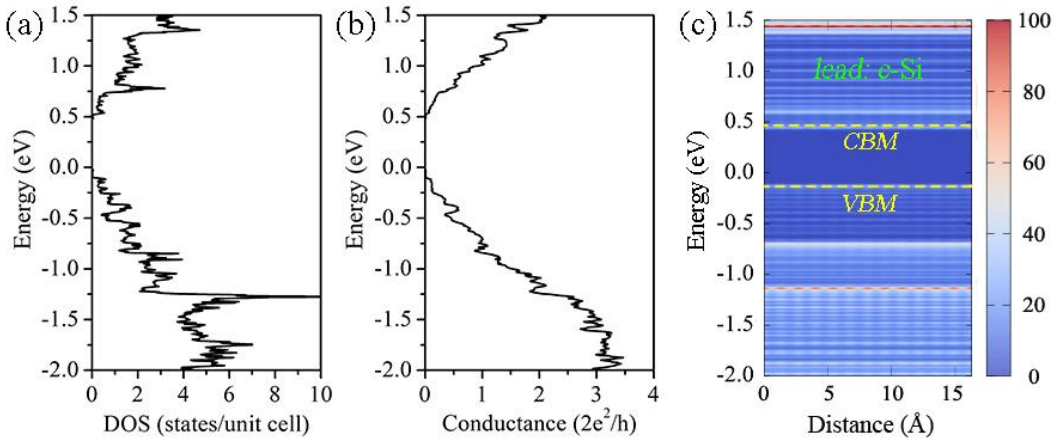

Fig. S2. (a) Spatially integrated density of states, (b) quantum conductance and (c) layer-resolved density of states of *c*–Si along the [001] direction. The valence band maximum and conduction band minimum are highlighted in dashed yellow lines.

Since only the bands around the gap will effectively be involved in the electronic transport, we examine the layer-resolved density of states (LRDOS) of *c*–Si to determine the band edges around the Fermi level. A downshift of 6 eV is applied in Fig. S2c in order to match the electronic band structure. In this condition, the valence band maximum (VBM) is computed to be at –0.10 eV and the conduction band minimum (CBM) is at 0.53 eV. In Fig. S2c, the band edges are highlighted in dashed yellow lines. We found that the gap between the VBM and CBM in LRDOS is ~0.63 eV, which is in good agreement with the transmission gap of 0.62 eV.

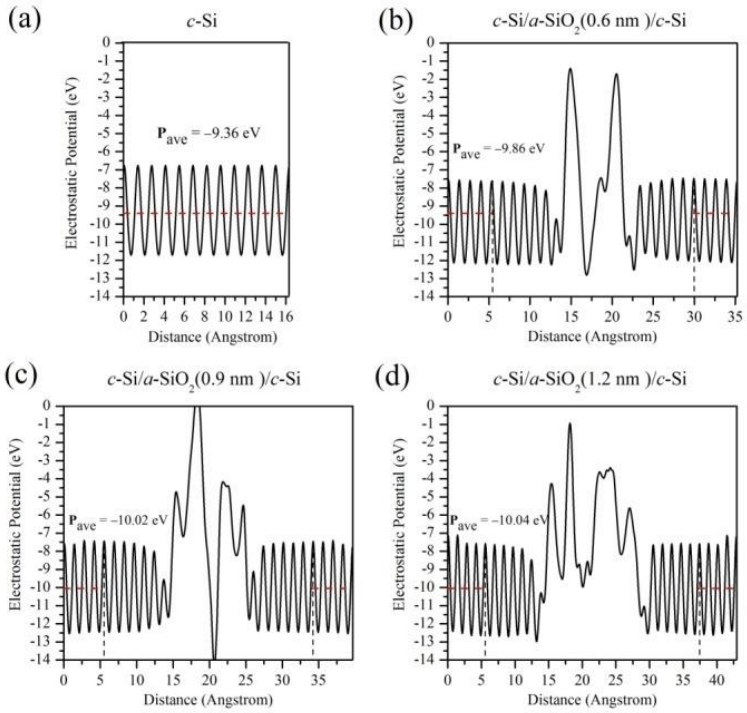

Fig. S3. Electrostatic potential of (a) the *c*–Si lead and the buffer layer in the *c*–Si/*a*–SiO_2/*c*–Si sandwich structures with thicknesses of (b) 0.6, (c) 0.9 and (c) 1.2 nm *a*–SiO_2 tunnel oxide layer.

Reference

(1) Marzari, N.; Mostofi, A. A.; Yates, J. R.; Souza, I.; Vanderbilt, D., Maximally Localized Wannier Functions: Theory and Applications. *Rev. Mod. Phys.* **2012**, *84*, 1419-1475.

(2) Calzolari, A.; Marzari, N.; Souza, I.; Nardelli, M. B., Ab Initio Transport Properties of Nanostructures from Maximally Localized Wannier Functions. *Phys. Rev. B* **2004**, *69*, 035108.

(3) Want Code by A. Ferretti, B. Bonferroni, A. Calzolari, and M. Buongiorno Nardelli, Http://Www.Wannier-Transport.Org.

(4) Souza, I.; Marzari, N.; Vanderbilt, D., Maximally Localized Wannier Functions for Entangled Energy Bands. *Phys. Rev. B* **2001**, *65*, 035109.

(5) Landauer, R., Electrical Resistance of Disordered One-Dimensional Lattices. *Philos. Mag.* **1970**, *21*, 863-867.

(6) Ferretti, A.; Calzolari, A.; Bonferroni, B.; Di Felice, R., Maximally Localized Wannier Functions Constructed from Projector-Augmented Waves or Ultrasoft Pseudopotentials. *J Phys-Condens Mat* **2007**, *19*.

(7) Fisher, D. S.; Lee, P. A., Relation between Conductivity and Transmission Matrix. *Phys. Rev. B* **1981**, *23*, 6851-6854.